
Wavelet Meets Adam: Compressing Gradients for Memory-Efficient Training

Ziqing Wen¹, Ping Luo¹, Jiahuan Wang¹, Jinping Zou¹, Xiaoge Deng²,
Kun Yuan³, Dongsheng Li¹, Tao Sun^{1*}

¹College of Computer Science and Technology, National University of Defense Technology.

²Intelligent Game and Decision Lab, Beijing, China.

³Center for Machine Learning Research, Peking University.

{zqwen, pingluo, wangjiahuan, zoujinping, dsli}@nudt.edu.cn;
dengxg@ustc.edu; kunyuan@pku.edu.cn; nudtsuntao@163.com

Abstract

Large language models (LLMs) have shown impressive performance across a range of natural language processing tasks. However, their vast number of parameters introduces significant memory challenges during training, particularly when using memory-intensive optimizers like Adam. Existing memory-efficient algorithms often rely on techniques such as singular value decomposition projection or weight freezing. While these approaches help alleviate memory constraints, they generally produce suboptimal results compared to full-rank updates. In this paper, we investigate the memory-efficient method beyond low-rank training, proposing a novel solution called Gradient Wavelet Transform (GWT), which applies wavelet transforms to gradients in order to significantly reduce the memory requirements for maintaining optimizer states. We demonstrate that GWT can be seamlessly integrated with memory-intensive optimizers, enabling efficient training without sacrificing performance. Through extensive experiments on both pre-training and fine-tuning tasks, we show that GWT achieves performance comparable to advanced memory-efficient optimizers and full-rank approaches in terms of both memory usage and training performance.

1 Introduction

Large Language Models (LLMs) have made remarkable strides since the release of ChatGPT [2]. Their promising performance and scalability have led to rapid adoption across a range of interdisciplinary fields, including science [1, 27, 28], medicine [13, 29, 33, 49], and policy-making in biology [20]. The impressive capabilities of LLMs arise from their vast number of parameters and the massive datasets used for training. However, training these models imposes significant demands on the optimizer, with Adam [22] emerging as the most commonly used optimizer due to its fast convergence, robustness, and considerable experimental results.

Despite these advantages, Adam’s memory requirements present a major drawback. Specifically, it consumes twice the memory of the model itself (as illustrated in Figure 1), making memory usage a key bottleneck in LLM training. For instance, pre-training a LLaMA 7B [43] model requires approximately 58GB of GPU memory: 14GB for model weights, 14GB for gradients, 2GB for activations, and 28GB for Adam optimizer states under BF16 precision [54]. When the model size exceeds 100B parameters, as with GPT-3 [2] (175B parameters), the additional memory overhead from Adam can exceed 700GB, requiring at least 9 additional NVIDIA A100 80GB GPUs.

*Corresponding Authors.

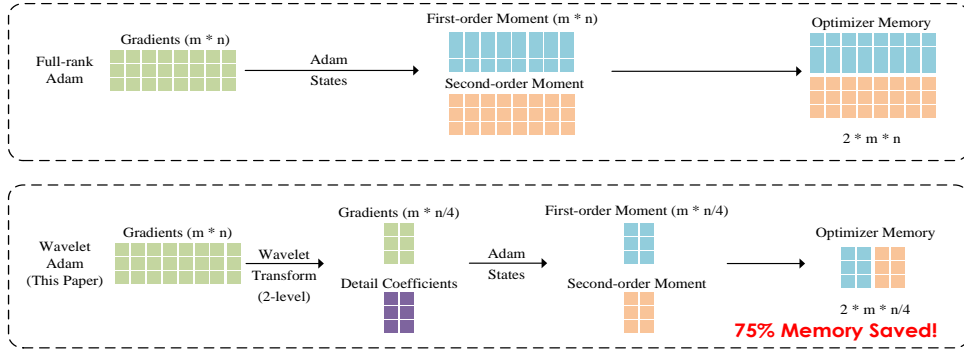


Figure 1: **Visualization of memory usage for Adam optimizer states.** Compared with full-rank Adam, the 2-level wavelet transform can reduce the optimizer state up to 75%.

Given the high costs of training LLMs, methods that reduce the batch size or use larger GPUs quickly become unsustainable. To mitigate these issues, many studies have focused on optimizing memory usage in LLM training. A promising solution is low-rank training [21, 54], which has made significant progress in alleviating memory constraints. These memory-efficient methods can be broadly classified into two categories: weight-based and gradient-based approaches [6]. Notable examples include Low-Rank Adaptation (LoRA) [21] and Gradient Low-Rank Projection (GaLore) [54].

LoRA leverages the low-rank nature of model parameter updates by freezing the pre-trained model weights and reparameterizing weight updates with trainable low-rank decomposition matrices. Extensive experiments have demonstrated that LoRA is effective in fine-tuning tasks, but its performance in pre-training remains limited. Additionally, the strong low-rank assumptions underlying LoRA often lead to suboptimal outcomes [50, 52]. FLoRA [16], on the other hand, uses resampling projection matrices to address the low-rank constraints of LoRA.

In contrast to LoRA, which decomposes the update matrix, GaLore reduces the optimizer state memory usage by performing Singular Value Decomposition (SVD) on the gradients, since the memory occupied by optimizer states is directly tied to the gradient size (as shown in Figure 1). GaLore has demonstrated effective performance in both pre-training and fine-tuning tasks. However, its performance still lags behind that of full-rank methods, and it only captures information within the projected subspace, discarding gradient information outside of it. This limitation becomes particularly problematic when using lower ranks or when gradients are noisy [6, 17].

To address these challenges, Fira [6] introduces the error residual between the full-rank gradient and its subspace projection, while GoLore [17] enhances GaLore by utilizing random projection to better capture gradient information when noise is dominant. However, these methods still rely on SVD for updating the subspace, and the high computational cost of SVD ($O(m \times n^2)$ for a matrix of size $m \times n$) can significantly slow down training, particularly for large models. To mitigate this issue, APOLLO [56] proposes an SVD-free variant of GaLore, replacing SVD with random projections. This modification not only improves training speed but also leads to enhanced empirical performance.

While it is intuitive to expect that information loss in low-rank approximations would degrade performance relative to full-rank training, extensive experiments have shown otherwise: both Fira and APOLLO have **surprisingly outperformed full-rank training** in various settings. These findings underscore the potential of memory-efficient optimization algorithms as strong alternatives to full-rank methods, making efficient training not only necessary but also advantageous in practice.

The above methods are based on low-rank decomposition. Aside from low-rank decomposition, the Wavelet Transform (WT) also has wide applications in the field of compression. Compared with low-rank decomposition, wavelet transform has lower computational complexity ($O(m \times n)$), better captures local information features, and suppresses high-frequency noise [37]. Moreover, due to its robustness to noise, it is better suited for stochastic gradient descent, a training model method that involves noise. Therefore, we can naturally raise the following question:

Can wavelet decomposition, like SVD, benefit the training of large language models, reducing memory consumption and improving model performance?

To address the limitations of existing low-rank training methods, we introduce Gradient Wavelet Transform (GWT), a simple yet effective plug-and-play framework that applies wavelet transforms to gradients during training. By leveraging the natural sparsity and localization properties of wavelets, GWT compresses gradient representations and significantly reduces the memory required to store optimizer states without relying on low-rank assumptions. Distinct from traditional matrix-based compression techniques, GWT is the first method to adopt a frequency-domain perspective for gradient compression. It achieves memory efficiency by selectively controlling low- and high-frequency coefficients. When applied to large-scale language model pretraining, such as LLaMA on the C4 dataset, GWT achieves up to 71% optimizer memory reduction and 1.9× training speedup on 3B models, all while maintaining or even improving model quality. Moreover, GWT integrates seamlessly with optimizers beyond Adam, highlighting its versatility across different training regimes. These results demonstrate that GWT provides a **practical, optimizer-agnostic, and highly efficient solution** for memory-constrained deep learning.

2 Related Works

Memory-Efficient Optimizers. Given the high memory requirements of the Adam optimizer [22], numerous approaches aim to improve the optimizer or create new optimization methods to reduce training costs for LLMs. Low-Rank Adaptation (LoRA) [21], which addresses this issue by freezing the parameters of the pre-trained model and introducing trainable low-rank matrices that decompose the pre-trained weights. LoRA has proven to be an effective strategy for optimizing the training of large language models, and several subsequent studies have built upon this framework to further enhance optimization performance [16, 23, 50, 52]. Gradient Low-Rank Projection (GaLore) [54] lowers the memory cost of optimizer states by projecting gradients into a lower-dimensional subspace. This method not only facilitates full-parameter LLM training but also delivers strong performance in both pretraining and fine-tuning tasks. Recent GaLore-based extensions have shown experimental results that outperform full-rank methods [6, 56].

System Memory Efficiency. Beyond optimizing memory usage at the level of the optimizer, some strategies target reducing memory consumption in the overall system. Gradient checkpointing [5] is one such method that conserves memory by not storing activation values. Memory offloading [35] improves memory availability during training by utilizing non-GPU memory resources. Quantization techniques [8, 9] further reduce memory overhead by employing lower-bit data representations. These methods have significantly accelerated and optimized LLM training processes. Our GWT approach offers a distinct advantage over these techniques by providing a memory-efficient alternative. Moreover, our method is designed to be compatible with existing system-level optimization strategies, allowing for a synergistic integration that can lead to even faster and more efficient LLM training.

3 Methods

In this section, we first provide an overview of the fundamental theory behind wavelet transforms, followed by a detailed explanation of how the proposed Gradient Wavelet Transform (GWT) method is integrated into the Adam optimizer [22].

3.1 Discrete Haar Wavelet Transform

Wavelet transforms can be categorized into continuous and discrete types. In this paper, we mainly focus on the discrete Haar wavelet due to its simple and easy-to-understand basis functions, high computational efficiency, broad applicability to compression tasks [32], and the fact that the total amount of data after decomposition equals the original data, without introducing extra information. It decomposes a signal (or image) into two main components: (a) Approximation coefficients (low-frequency), which represent the smooth or average part of the signal/image, and (b) Detail coefficients (high-frequency), which capture the finer details or differences in the signal/image.

For example, for an input signal or image represented by the sequence of values $[x_1, x_2, x_3, x_4, x_5, x_6, x_7, x_8]$, the 1-level Discrete Haar Transform (DHT, Haar-1) computes the Approximation and Detail coefficients as follows

$$A_1 = \left[\frac{x_1 + x_2}{\sqrt{2}}, \frac{x_3 + x_4}{\sqrt{2}}, \frac{x_5 + x_6}{\sqrt{2}}, \frac{x_7 + x_8}{\sqrt{2}} \right], D_1 = \left[\frac{x_1 - x_2}{\sqrt{2}}, \frac{x_3 - x_4}{\sqrt{2}}, \frac{x_5 - x_6}{\sqrt{2}}, \frac{x_7 - x_8}{\sqrt{2}} \right].$$

The wavelet filter for DHT are $[\frac{1}{\sqrt{2}}, \frac{1}{\sqrt{2}}]$ for approximation, and $[\frac{1}{\sqrt{2}}, -\frac{1}{\sqrt{2}}]$ for detail coefficients. The reconstruction of the original signal can be expressed as follows

$$[x_1, x_3, x_5, x_7] = \frac{A_1 + D_1}{\sqrt{2}}, [x_2, x_4, x_6, x_8] = \frac{A_1 - D_1}{\sqrt{2}}. \quad (1)$$

Next, we can apply an additional DHT transform to the approximation coefficient A_1 , yielding the following results:

$$A_2 = \left[\frac{x_1 + x_2 + x_3 + x_4}{2}, \frac{x_5 + x_6 + x_7 + x_8}{2} \right], D_2 = \left[\frac{x_1 + x_2 - x_3 - x_4}{2}, \frac{x_5 + x_6 - x_7 - x_8}{2} \right].$$

Therefore, we have derived a simple implementation of 2-level DHT, the corresponding reconstruction is similar to 1-level. The DHT converts a vector with eight elements into two vectors (A_1, D_1) of 4 elements each or three vectors (A_2, D_2, D_1). Storing just approximation coefficients will reduce our memory cost by 50% or 75%. This process can be repeated iteratively, breaking the signal into increasingly finer levels of approximation and detail, facilitating efficient compression and storage.

Building on the derivation above, we can represent the Discrete DHT as a matrix projection. For a more general formulation, let $W \in \mathbb{R}^{m \times n}$ be a matrix (we suppose $n \bmod 2 = 0$ for simplicity). The DHT and reconstruction can be expressed as:

$$[A, D] = WH, \quad W = [A, D]H^T, \quad (2)$$

where $A, D \in \mathbb{R}^{m \times \frac{n}{2}}$, $H, \tilde{H} \in \mathbb{R}^{n \times n}$ denote the Haar wavelet transform matrix, and the elements are defined as:

$$H_{2i-1, i} = H_{2i, i} = H_{2i-1, \frac{n}{2}+i} = \frac{1}{\sqrt{2}}, H_{2i, \frac{n}{2}+i} = -\frac{1}{\sqrt{2}} \quad (3)$$

It is straightforward that $HH^T = I$, where I is the identity matrix. For higher-level DHT, the formulation is similar. This matrix-based representation allows for efficient computation and generalization of the DHT to higher-dimensional cases, making it a powerful tool for applications such as gradient compression in optimization methods.

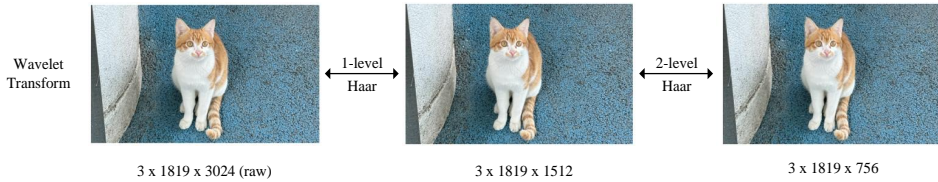


Figure 2: **Visualization of the approximation coefficients of a 2-Level DHT on an image (rescaled for visual clarity).** Even after reducing the image to 25% of its original size (right), the approximation coefficients successfully preserve the key structural features of the image.

3.2 Adam with GWT

The Adam optimizer [22] adaptively adjusts the learning rates for each parameter based on its past gradient states, while also incorporating momentum to accelerate training. The update rule for the weights is given by the following recursive equation:

$$W_{t+1} = W_t - \eta \cdot \tilde{G}_t, \tilde{G}_t = \frac{M_t}{\sqrt{V_t} + \epsilon} \quad (4)$$

Algorithm 1 Adam with Wavelet Transform

Input: Weight matrix W , step size η , batch size m , decay rates β_1, β_2 , iteration T , ϵ for numerical stability, scale factor α , wavelet transform level l , and wavelet transformer H^l .

Initialize $t \leftarrow 0$

repeat

$$G_t \leftarrow \frac{1}{m} \sum_{i=1}^m \nabla_W f_i(W_t) \quad \triangleright \text{Batch gradient}$$

$$[A_t, D_t] \leftarrow G_t H^l \quad \triangleright \text{Gradient wavelet transform}$$

if $t = 0$ **then**

 Initialize $M_{-1}, V_{-1} \leftarrow 0$

end if

Adam states update

$$M_t^R \leftarrow \beta_1 \cdot M_{t-1}^R + (1 - \beta_1) \cdot A_t$$

$$V_t^R \leftarrow \beta_2 \cdot V_{t-1}^R + (1 - \beta_2) \cdot A_t^2$$

$$[\tilde{A}_t, \tilde{D}_t] \leftarrow [M_t^R / (\sqrt{V_t^R} + \epsilon), D_t / (\sqrt{V_t^R} + \epsilon)]$$

$$\tilde{G}_t \leftarrow \alpha \cdot [\tilde{A}_t, \tilde{D}_t] H^T \quad \triangleright \text{Wavelet transform back}$$

$$\eta_t \leftarrow \eta \cdot \frac{\sqrt{1 - \beta_2^t}}{(1 - \beta_1^t)} \quad \triangleright \text{Bias correction}$$

$$W_t \leftarrow W_{t-1} - \eta_t \cdot \tilde{G}_t \quad \triangleright \text{Update weights}$$

$t \leftarrow t + 1$

until $t = T$

return W_t

where $\eta > 0$ denotes the learning rate, \cdot represents the element-wise multiplication, $W \in \mathbb{R}^{m \times n}$ and

$$M_t = \beta_1 \cdot M_{t-1} + (1 - \beta_1) \cdot G_t, V_t = \beta_2 \cdot V_{t-1} + (1 - \beta_2) \cdot G_t^2. \quad (5)$$

Here, $\beta_1, \beta_2 \in [0, 1)$ are the decay rates hyperparameters which are set as 0.9, 0.999 commonly, $\epsilon > 0$ to preserve numerical stability, $G_t \in \mathbb{R}^{m \times n}$ denotes the batch gradient at time step t , and $M, V \in \mathbb{R}^{m \times n}$ represents the first/second-order moment in Adam optimizer.

For ease of presentation, we adopt a 1-level DHT in the following discussion. To integrate GWT with the Adam optimizer, we begin by applying GWT to the gradient matrix G_t at time step t (Eq. (2)), focusing on the approximate coefficients. This results in a compressed gradient matrix (approximation coefficient) $A_t \in \mathbb{R}^{m \times \frac{n}{2}}$ and a detail coefficient matrix $D_t \in \mathbb{R}^{m \times \frac{n}{2}}$. We then update the Adam states by replacing the original gradient G_t in the update rule (Eq. (5)) with the smaller matrix A_t to calculate \tilde{G}_t . To preserve the consistency of the state update, we scale the wavelet detail coefficients D_t by dividing them by D_t by $\sqrt{V_t^R} + \epsilon$ based on the linear properties of DHT (Eq. (2)). Finally, project \tilde{G}_t back to the original space and update the weights. The update rule can be rewritten as follows if we have $[A_t, D_t] = G_t H$,

$$M_t^R = \beta_1 \cdot M_{t-1}^R + (1 - \beta_1) A_t, V_t^R = \beta_2 V_{t-1}^R + (1 - \beta_2) A_t^2, \quad (6)$$

then compute the normalized coefficients by

$$\tilde{A}_t = \frac{M_t^R}{\sqrt{V_t^R} + \epsilon}, \tilde{D}_t = \frac{D_t}{\sqrt{V_t^R} + \epsilon}.$$

Therefore, we can update the weight in the original space

$$\tilde{G}_t = [\tilde{A}_t, \tilde{D}_t] H^T, W_{t+1} = W_t - \eta_t \cdot \tilde{G}_t$$

The procedure for applying GWT to the Adam optimizer is outlined in Algorithm 1. We implement the Adam optimizer with Haar-2 on the LLaMA 130M model, and present the learning curve in Figure 3. We observe that the learning curve (blue) demonstrates a twice spike around the 900th and 2500th iteration. This phenomenon is likely due to unstable gradients during the early stages of training, as observed in previous studies [6, 30]. To address this issue, we adopt the Norm-growth Limiter (NL) technique introduced by Fira [6], which stabilizes gradient growth. NL controls the

ratio of the current gradient norm to the previous gradient norm by rescaling the current gradient as follows

$$\text{if } \frac{\|\tilde{G}_t\|}{\|\tilde{G}_{t-1}\|} > \gamma \text{ then } \tilde{G}_t \leftarrow \frac{\tilde{G}_t}{\|\tilde{G}_t\|} \cdot \gamma \cdot \|\tilde{G}_{t-1}\|,$$

where γ is a threshold that limits the gradient norm growth, we adopt $\gamma = 1.01$ by default. This technique significantly reduces the impact of unstable gradients in the early training stages [56]. After introducing NL, the learning curve (orange) for our Haar-2 implementation becomes smoother, resulting in a lower training loss.

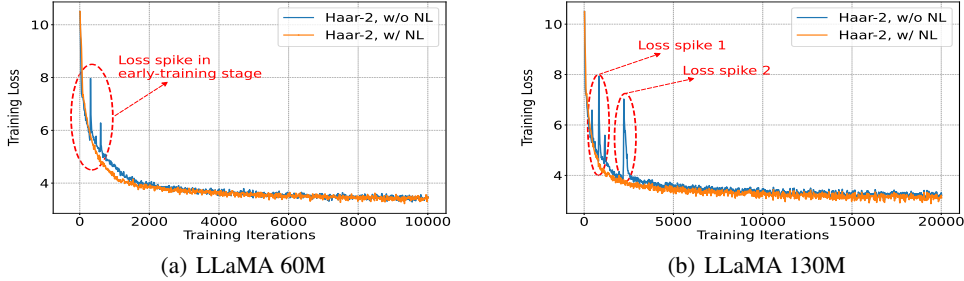


Figure 3: **Training loss comparison between Haar-2 with/without NL on LLaMA 60M and 130M.**

In summary, we integrate the proposed GWT method into the Adam optimizer and observe that it can theoretically reduce the memory footprint of optimizer states by up to 75%. GWT achieves this by projecting gradients into a lower-dimensional subspace and performing updates to the optimizer states within this subspace. This memory-efficient strategy significantly reduces the storage requirements and can be applied to a wide range of optimizers that maintain substantial state information.

Importantly, the GWT is not limited to Adam. In Appendix F, we present a unified formulation for extending GWT to other memory-intensive optimizers. We also provide empirical results demonstrating that GWT, when integrated with optimizers such as Adam-mini [53] and MUON [24], achieves comparable performance to those optimizers.

4 Experiments

In this section, we demonstrate that the Gradient Wavelet Transform (GWT), as a memory-efficient optimization technique, can achieve performance comparable to or even surpassing that of full-rank optimizers, while significantly reducing memory usage and increasing training throughput. Specifically, we evaluate GWT in two contexts: pre-training LLaMA [43] models on the Colossal Clean Crawled Corpus (C4) [34] English benchmark, fine-tuning various pre-trained models on the Multi-task Language Understanding (MMLU) [18] and RoBERTa-base on the General Language Understanding Evaluation (GLUE) [45] benchmarks. We adopt the BF-16 format to reduce memory usage across all experiments and provide a detailed description of these datasets in Appendix G.

For GWT, we use the discrete Haar wavelet as the default filter. Additionally, we present an ablation study to examine the impact of key hyperparameters, including the scale factor (α), initial learning rate (lr), the GWT level (l), and other wavelet bases, as detailed in Appendix A.2. A comprehensive description of the experimental setup can be found in Appendix A.

4.1 Memory-Efficient Pre-Training

We integrate our proposed GWT method into the Adam optimizer [22], using default hyperparameters ($\beta_1 = 0.9$, $\beta_2 = 0.999$, $\epsilon = 10^{-6}$), and evaluate its performance on the LLaMA models using the C4 pretraining task. To provide a comprehensive comparison, we include our reproduced results for full-rank Adam [22], GaLore [54], and APOLLO [56], alongside reference results reported by Fira [6], and LoRA [54]. All experiments adopt a consistent configuration: we use GaLore’s default hyperparameters ($lr = 0.01$, $\alpha = 0.25$) for both GaLore and GWT, and $\alpha = 1.0$ for APOLLO. A

Table 1: **Final validation PPL (lower is better) and estimated memory usage on pre-training LLaMA models on the C4 dataset.** We use GWT-2 to denote the Adam optimizer equipped with a 2-level Haar GWT. Notably, GWT, APOLLO, and Fira all demonstrate performance surpassing that of the full-rank method. As shown, GWT consistently outperforms baseline methods, achieving comparable or even lower validation perplexity while using significantly less memory. Results marked with * indicate values reported in previous works.

Methods	60M	130M	350M	1B
Full-Rank Adam	33.37 (0.36G)	25.08 (0.76G)	18.75 (2.06G)	16.10 (7.80G)
GWT-2	29.35 (0.24G)	22.47 (0.52G)	16.29 (1.22G)	13.50 (4.38G)
GaLore-1/4	39.94 (0.24G)	26.47 (0.52G)	19.36 (1.22G)	15.66 (4.38G)
APOLLO-1/4	31.53 (0.24G)	23.35 (0.52G)	16.73 (1.22G)	14.10 (4.38G)
GWT-3	29.81 (0.22G)	22.63 (0.48G)	16.35 (1.08G)	13.48 (3.81G)
GaLore-1/8	48.48 (0.22G)	30.02 (0.48G)	21.59 (1.08G)	17.52 (3.81G)
APOLLO-1/8	32.50 (0.22G)	23.74 (0.48G)	16.98 (1.08G)	14.32 (3.81G)
Fira* [6]	31.06 (0.24G)	22.73 (0.52G)	17.03 (1.22G)	14.31 (4.38G)
LoRA* [54]	34.99 (0.36G)	33.92 (0.80G)	25.58 (1.76G)	19.21 (6.17G)
Training Tokens	1.3B	2.6B	7.8B	13.1B

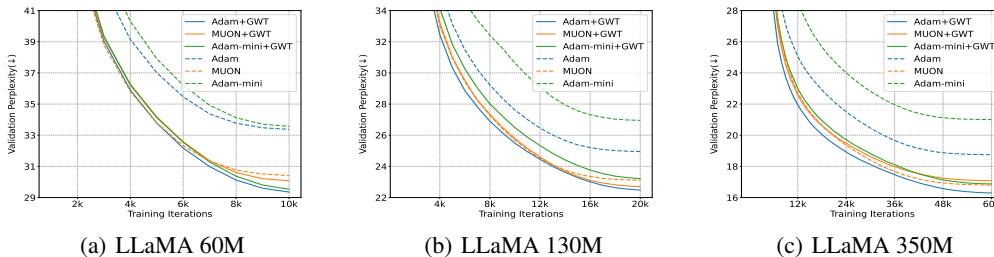


Figure 4: **Applying GWT to Adam/Adam-mini/MUON optimizers for pre-training various LLaMA models.** GWT is scalable to optimizers beyond Adam and consistently achieves lower or comparable PPL than full-rank methods across all tested optimizers.

cosine annealing schedule is applied to the learning rate. We use a sequence length of 256 and a batch size of 512, resulting in a total of 131K tokens per batch, unless stated otherwise.

For GaLore-r and APOLLO-r, we experiment with compression ratios corresponding to 1/4 and 1/8 of the model rank, denoted as GaLore-1/4 and GaLore-1/8, respectively. These settings are aligned with GWT configurations using 2- and 3-level decompositions. Following prior work [54], we apply the same network initialization strategy and enable GWT in both the Multi-Layer Perceptron (MLP) and attention modules of the transformer.

GWT is effective in pre-training. The final validation perplexity (PPL) and estimated memory usage for all methods are summarized in Table 1. Experimental results show that GWT consistently achieves lower validation PPL while reducing memory usage compared to other memory-efficient baselines. In all the pre-training cases, GWT outperforms full-rank optimizers. Specifically, in the LLaMA 1B pre-training experiment, our 2-level GWT method reduces the total memory cost by 51% and the optimizer memory cost by 76% (from 7.80GB to 3.81GB on LLaMA 1B). Even with the use of 2-level GWT, our method still achieves experimental results that surpass full-rank, while reducing total memory consumption by up to 43%. In the same scenario, the gap between GaLore-1/8 and full-rank is further widened. Details of the memory estimation are presented in Appendix A.4.

GWT leads to faster convergence. We present learning curves for the pre-training task on LLaMA 60M-350M in Figure 4. These curves show that GWT consistently outperforms both full-rank Adam and GaLore across different levels of wavelet transformation. In most cases, GaLore consistently shows a significant gap compared to full-rank Adam, while all GWT methods maintain results

surpassing full-rank. Moreover, GWT not only achieves lower final validation PPL but also accelerates convergence compared to the baselines.

GWT is optimizer-agnostic. We extend our method to the Adam-mini [53] and MUON [24] optimizers and present the corresponding experimental results in Figure 4. Similar to its performance with Adam, GWT continues to achieve results comparable to or better than the full-rank methods. This highlights the versatility and effectiveness of our method when integrated with other optimizers, showcasing its broad applicability in memory-efficient optimization.

Table 2: **Pre-training LLaMA 3B on C4.** We report the validation PPL on different iterations and the training token throughput per GPU (RTX 3090).

	20K	40K	60K	80K	100K	120K	Tokens/s	Mem.
GaLore-1/4	21.60	17.85	16.95	15.93	15.34	15.02	0.506K	8.54G
APOLLO-1/4	20.73	17.01	15.26	14.41	14.03	13.88	0.541K	8.54G
8bit-Adam	21.89	18.01	17.12	15.99	15.45	15.20	0.274K	10.7G
GWT-2	19.74	16.41	14.80	13.77	13.46	13.31	0.532K	8.54G
Tokens (B)	2.6	5.2	7.8	10.4	13.1	15.7		

GWT achieves higher training throughput. In addition to evaluating final validation perplexity and memory consumption, we also measure token throughput during the pretraining of the LLaMA-3B model using GWT-2, GaLore-1/4, APOLLO-1/4, and 8-bit Adam. The results are presented in Table 2. Our method, GWT-2, achieves a training throughput of 0.532K tokens per second per GPU, delivering over a 1.9 \times speedup compared to 8-bit Adam [8], and approximately a 6% improvement over GaLore. Furthermore, GWT-2 achieves throughput comparable to the SVD-free APOLLO method, highlighting its efficiency in large-scale model training.

GWT is robust to long sequence lengths. We evaluate GWT in handling longer sequences (512, 1024) while keeping the total number of training tokens per batch constant. Table 3 reports the final validation PPL across different methods. In contrast to GaLore, which exhibits noticeable performance degradation as sequence length increases, GWT maintains stable performance, showing only a slight increase in PPL. This resilience highlights GWT as a promising candidate for partial LLM pre-training scenarios, i.e., long-context windows and trillions of training tokens.

Table 3: **Final validation PPL on pre-training LLaMA models with different sequence length.**

Models	60M		130M		350M	
Sequence length	512	1024	512	1024	512	1024
Full-Rank Adam	34.55	37.52	25.95	28.12	19.95	22.02
GaLore-1/4	40.25	42.02	27.19	33.97	19.92	21.73
APOLLO-1/4	32.29	34.64	24.02	25.93	17.26	18.77
GWT-2	30.12	32.55	23.01	24.89	16.68	18.21

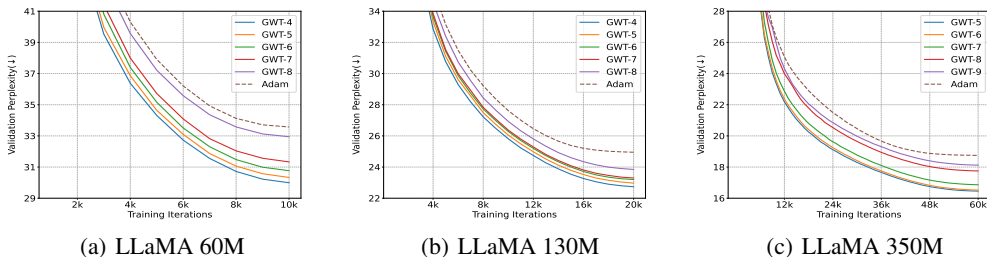


Figure 5: **Applying GWT to Adam for pre-training LLaMA models with reduced memory usage (higher l).** GWT maintains superior performance over Adam under high wavelet transform l levels.

Table 4: **Comparison results of various fine-tuning algorithms on MMLU tasks.** GWT maintains accuracy comparable to Full-rank Adam or other memory-efficient algorithms across different models.

Models	Methods	STEM	Social Sciences	Humanities	Other	Avg.
LLaMA3.2-3B	Adam	49.50	68.25	56.28	64.74	59.40
	LoRA	49.83	67.63	56.56	63.88	59.23
	GaLore	49.73	68.70	55.94	64.47	59.37
	APOLLO	49.17	68.18	56.32	64.71	59.32
	GWT	49.50	68.61	56.56	64.62	59.34
Gemma3-4B	Adam	46.59	64.74	49.71	58.91	54.46
	LoRA	45.36	63.41	48.63	58.36	53.41
	GaLore	46.36	64.51	49.42	58.91	54.26
	APOLLO	46.49	64.28	49.39	58.67	54.17
	GWT	46.39	64.87	49.73	59.38	54.56
Qwen2.5-7B	Adam	-	-	-	-	OOM
	LoRA	70.44	83.23	67.80	76.90	73.85
	GaLore	70.21	83.49	67.52	76.87	73.76
	APOLLO	70.51	83.43	67.35	76.96	73.77
	GWT	70.38	83.88	68.06	77.14	74.12

GWT remains efficient under SGD-level memory constraints. We assess the performance of GWT at higher decomposition levels, as illustrated in Figure 5. Notably, even at extreme levels (e.g., $l = 7, 8, 9$), where the memory footprint of the optimizer approaches that of SGD, GWT consistently outperforms full-rank Adam in terms of validation PPL, demonstrating its robustness and effectiveness in low-memory training regimes.

4.2 Memory-Efficient Fine-Tuning

In this section, we further evaluate the effectiveness of our method by fine-tuning the LLaMA-3.2-3B [15], Gemma3-4B [41], and Qwen2.5-7B [51] models, and report their performance on the MMLU benchmark [18]. For a fair comparison, LoRA, GaLore, and APOLLO are configured with a rank of 8, while GWT is set to a decomposition level of 8 to ensure memory alignment across methods. We report the best accuracy achieved by sweeping the learning rate over the range [1.0e-6, 2.5e-6, 5.0e-6, 1.0e-5, 2.5e-5, 5.0e-5, 1.0e-4], which covers a sufficiently broad span and ensures a fair evaluation for optimizers with different sensitivities to learning rates. Additionally, to provide a more comprehensive assessment, we include results from fine-tuning the RoBERTa-base model [25] on the GLUE benchmark, as presented in Appendix B.

GWT is effective in fine-tuning. We report the MMLU results in Table 4 and the GLUE results in Table 10. As shown, GWT consistently matches or exceeds the performance of other memory-efficient baselines. These results demonstrate that GWT is not only effective during pre-training but also excels in fine-tuning scenarios, achieving competitive performance across diverse tasks while maintaining memory efficiency.

5 Conclusion

In this paper, we explore memory-efficient optimization algorithms that go beyond traditional low-rank decomposition and system-level techniques. Drawing inspiration from the limitations of current optimization methods and the demonstrated success of WT in image and signal processing, we propose a novel optimizer state memory compression method that integrates WT into gradients. This method bridges the gap between gradient compression and wavelet transforms, enabling more efficient training of LLMs by reducing memory usage and accelerating training speed.

Our experimental results demonstrate that GWT achieves performance comparable to that of advanced memory-efficient optimizers and full-rank methods across various LLM training stages. This gradient

compression technique not only improves final validation scores but also accelerates training convergence and increases throughput. Moreover, this method is applicable to existing memory-intensive optimizers beyond Adam. In summary, our approach validates the feasibility of applying wavelet transforms to enhance the training efficiency of LLMs, providing a novel perspective on designing memory-efficient algorithms that effectively address the memory bottleneck in LLMs training.

References

- [1] D. A. Boiko, R. MacKnight, B. Kline, and G. Gomes. Autonomous chemical research with large language models. *Nature*, 624(7992):570–578, 2023.
- [2] T. B. Brown, B. Mann, N. Ryder, M. Subbiah, J. Kaplan, P. Dhariwal, A. Neelakantan, P. Shyam, G. Sastry, A. Askell, S. Agarwal, A. Herbert-Voss, G. Krueger, T. Henighan, R. Child, A. Ramesh, D. M. Ziegler, J. Wu, C. Winter, C. Hesse, M. Chen, E. Sigler, M. teusz Litwin, S. Gray, B. Chess, J. Clark, C. Berner, S. McCandlish, A. Radford, I. Sutskever, and D. Amodei. Language models are few-shot learners. *ArXiv*, abs/2005.14165, 2020.
- [3] D. M. Cer, M. T. Diab, E. Agirre, I. Lopez-Gazpio, and L. Specia. Semeval-2017 task 1: Semantic textual similarity multilingual and crosslingual focused evaluation. In *International Workshop on Semantic Evaluation*, 2017.
- [4] H. Chen, G. Raskutti, and M. Yuan. Non-convex projected gradient descent for generalized low-rank tensor regression. *J. Mach. Learn. Res.*, 20:5:1–5:37, 2016.
- [5] T. Chen, B. Xu, C. Zhang, and C. Guestrin. Training deep nets with sublinear memory cost. *arXiv preprint arXiv:1604.06174*, 2016.
- [6] X. Chen, K. Feng, C. Li, X. Lai, X. Yue, Y. Yuan, and G. Wang. Fira: Can we achieve full-rank training of llms under low-rank constraint? *ArXiv*, abs/2410.01623, 2024.
- [7] Y. Chen and M. J. Wainwright. Fast low-rank estimation by projected gradient descent: General statistical and algorithmic guarantees. *ArXiv*, abs/1509.03025, 2015.
- [8] T. Dettmers, M. Lewis, S. Shleifer, and L. Zettlemoyer. 8-bit optimizers via block-wise quantization. *arXiv preprint arXiv:2110.02861*, 2021.
- [9] T. Dettmers, A. Pagnoni, A. Holtzman, and L. Zettlemoyer. Qlora: Efficient finetuning of quantized llms. *Advances in Neural Information Processing Systems*, 36, 2024.
- [10] W. B. Dolan and C. Brockett. Automatically constructing a corpus of sentential paraphrases. In *International Joint Conference on Natural Language Processing*, 2005.
- [11] A. Dosovitskiy, L. Beyer, A. Kolesnikov, D. Weissenborn, X. Zhai, T. Unterthiner, M. Dehghani, M. Minderer, G. Heigold, S. Gelly, J. Uszkoreit, and N. Houlsby. An image is worth 16x16 words: Transformers for image recognition at scale. *ICLR*, 2021.
- [12] K. Everett, L. Xiao, M. Wortsman, A. Alemi, R. Novak, P. J. Liu, I. Gur, J. N. Sohl-Dickstein, L. P. Kaelbling, J. Lee, and J. Pennington. Scaling exponents across parameterizations and optimizers. *ArXiv*, abs/2407.05872, 2024.
- [13] D. Ferber, G. Wölflein, I. C. Wiest, M. Ligerio, S. Sainath, N. Ghaffari Laleh, O. S. El Nahhas, G. Müller-Franzes, D. Jäger, D. Truhn, et al. In-context learning enables multimodal large language models to classify cancer pathology images. *Nature Communications*, 15(1):10104, 2024.
- [14] R. Genet and H. Inzirillo. Caadam: Improving adam optimizer using connection aware methods. *ArXiv*, abs/2410.24216, 2024.
- [15] A. Grattafiori, A. Dubey, A. Jauhri, A. Pandey, A. Kadian, A. Al-Dahle, A. Letman, A. Mathur, A. Schelten, A. Vaughan, et al. The llama 3 herd of models. *arXiv preprint arXiv:2407.21783*, 2024.
- [16] Y. Hao, Y. Cao, and L. Mou. Flora: Low-rank adapters are secretly gradient compressors. *arXiv preprint arXiv:2402.03293*, 2024.

- [17] Y. He, P. Li, Y. Hu, C. Chen, and K. Yuan. Subspace optimization for large language models with convergence guarantees. *arXiv preprint arXiv:2410.11289*, 2024.
- [18] D. Hendrycks, C. Burns, S. Basart, A. Zou, M. Mazeika, D. Song, and J. Steinhardt. Measuring massive multitask language understanding. *arXiv preprint arXiv:2009.03300*, 2020.
- [19] J. Ho, A. Jain, and P. Abbeel. Denoising diffusion probabilistic models. *Advances in neural information processing systems*, 33:6840–6851, 2020.
- [20] V. Hofmann, P. R. Kalluri, D. Jurafsky, and S. King. Ai generates covertly racist decisions about people based on their dialect. *Nature*, 633(8028):147–154, 2024.
- [21] E. J. Hu, Y. Shen, P. Wallis, Z. Allen-Zhu, Y. Li, S. Wang, L. Wang, and W. Chen. Lora: Low-rank adaptation of large language models. In *International Conference on Learning Representations*, 2022.
- [22] D. P. Kingma and J. Ba. Adam: A method for stochastic optimization. *CoRR*, abs/1412.6980, 2014.
- [23] V. Lialin, N. Shivagunde, S. Muckatira, and A. Rumshisky. Relora: High-rank training through low-rank updates. In *International Conference on Learning Representations*, 2023.
- [24] J. Liu, J. Su, X. Yao, Z. Jiang, G. Lai, Y. Du, Y. Qin, W. Xu, E. Lu, J. Yan, et al. Muon is scalable for llm training. *arXiv preprint arXiv:2502.16982*, 2025.
- [25] Y. Liu. Roberta: A robustly optimized bert pretraining approach. *arXiv preprint arXiv:1907.11692*, 364, 2019.
- [26] Z. Liu, Y. Lin, Y. Cao, H. Hu, Y. Wei, Z. Zhang, S. Lin, and B. Guo. Swin transformer: Hierarchical vision transformer using shifted windows. In *Proceedings of the IEEE/CVF international conference on computer vision*, pages 10012–10022, 2021.
- [27] D. Matthews, M. Spence, A. Mater, J. Nichols, S. Pulsford, M. Sandhu, J. Kaczmarski, C. Milton, N. Tokuriki, and C. Jackson. Leveraging ancestral sequence reconstruction for protein representation learning. *Nature Machine Intelligence*, 6(12):1542–1555, 2024.
- [28] O. Méndez-Lucio, C. A. Nicolaou, and B. Earnshaw. Mole: a foundation model for molecular graphs using disentangled attention. *Nature Communications*, 15(1):9431, 2024.
- [29] G. Mischler, Y. A. Li, S. Bickel, A. D. Mehta, and N. Mesgarani. Contextual feature extraction hierarchies converge in large language models and the brain. *Nature Machine Intelligence*, pages 1–11, 2024.
- [30] I. Molybog, P. Albert, M. Chen, Z. DeVito, D. Esiobu, N. Goyal, P. S. Koura, S. Narang, A. Poulton, R. Silva, B. Tang, D. Liskovich, P. Xu, Y. Zhang, M. H. M. Kambadur, S. Roller, and S. Zhang. A theory on adam instability in large-scale machine learning. *ArXiv*, abs/2304.09871, 2023.
- [31] A. Paszke, S. Gross, S. Chintala, G. Chanan, E. Yang, Z. DeVito, Z. Lin, A. Desmaison, L. Antiga, and A. Lerer. Automatic differentiation in pytorch. 2017.
- [32] P. Porwik and A. Lisowska. The haar-wavelet transform in digital image processing: Its status and achievements. *Machine graphics & vision*, 13:79–98, 2004.
- [33] P. Qiu, C. Wu, X. Zhang, W. Lin, H. Wang, Y. Zhang, Y. Wang, and W. Xie. Towards building multilingual language model for medicine. *Nature Communications*, 15(1):8384, 2024.
- [34] C. Raffel, N. M. Shazeer, A. Roberts, K. Lee, S. Narang, M. Matena, Y. Zhou, W. Li, and P. J. Liu. Exploring the limits of transfer learning with a unified text-to-text transformer. *J. Mach. Learn. Res.*, 21:140:1–140:67, 2019.
- [35] S. Rajbhandari, J. Rasley, O. Ruwase, and Y. He. Zero: Memory optimizations toward training trillion parameter models. In *SC20: International Conference for High Performance Computing, Networking, Storage and Analysis*, pages 1–16. IEEE, 2020.

- [36] P. Rajpurkar, R. Jia, and P. Liang. Know what you don't know: Unanswerable questions for squad. *ArXiv*, abs/1806.03822, 2018.
- [37] O. Rioul and M. Vetterli. Wavelets and signal processing. *IEEE Signal Processing Magazine*, 8(4):14–38, 1991.
- [38] R. Socher, A. Perelygin, J. Wu, J. Chuang, C. D. Manning, A. Ng, and C. Potts. Recursive deep models for semantic compositionality over a sentiment treebank. In *Conference on Empirical Methods in Natural Language Processing*, 2013.
- [39] Y. Song, J. Sohl-Dickstein, D. P. Kingma, A. Kumar, S. Ermon, and B. Poole. Score-based generative modeling through stochastic differential equations. In *International Conference on Learning Representations*, 2021.
- [40] R. Taori, I. Gulrajani, T. Zhang, Y. Dubois, X. Li, C. Guestrin, P. Liang, and T. B. Hashimoto. Stanford alpaca: An instruction-following llama model. https://github.com/tatsu-lab/stanford_alpaca, 2023.
- [41] G. Team, A. Kamath, J. Ferret, S. Pathak, N. Vieillard, R. Merhej, S. Perrin, T. Matejovicova, A. Ramé, M. Rivière, et al. Gemma 3 technical report. *arXiv preprint arXiv:2503.19786*, 2025.
- [42] H. Touvron, T. Lavril, G. Izacard, X. Martinet, M.-A. Lachaux, T. Lacroix, B. Rozière, N. Goyal, E. Hambro, F. Azhar, A. Rodriguez, A. Joulin, E. Grave, and G. Lample. Llama: Open and efficient foundation language models. *ArXiv*, abs/2302.13971, 2023.
- [43] H. Touvron, L. Martin, K. R. Stone, P. Albert, and e. a. Amjad Almahairi. Llama 2: Open foundation and fine-tuned chat models. *ArXiv*, abs/2307.09288, 2023.
- [44] A. Vaswani, N. M. Shazeer, N. Parmar, J. Uszkoreit, L. Jones, A. N. Gomez, L. Kaiser, and I. Polosukhin. Attention is all you need. In *Neural Information Processing Systems*, 2017.
- [45] A. Wang, A. Singh, J. Michael, F. Hill, O. Levy, and S. R. Bowman. Glue: A multi-task benchmark and analysis platform for natural language understanding. In *BlackboxNLP@EMNLP*, 2018.
- [46] A. Warstadt, A. Singh, and S. R. Bowman. Neural network acceptability judgments. *Transactions of the Association for Computational Linguistics*, 7:625–641, 2018.
- [47] A. Williams, N. Nangia, and S. R. Bowman. A broad-coverage challenge corpus for sentence understanding through inference. In *North American Chapter of the Association for Computational Linguistics*, 2017.
- [48] M. Wolter, F. Blanke, J. Garcke, and C. T. Hoyt. ptwt - the pytorch wavelet toolbox. *Journal of Machine Learning Research*, 25(80):1–7, 2024.
- [49] Z. Wu, O. Zhang, X. Wang, L. Fu, H. Zhao, J. Wang, H. Du, D. Jiang, Y. Deng, D. Cao, et al. Leveraging language model for advanced multiproperty molecular optimization via prompt engineering. *Nature Machine Intelligence*, pages 1–11, 2024.
- [50] W. Xia, C. Qin, and E. Hazan. Chain of lora: Efficient fine-tuning of language models via residual learning. *arXiv preprint arXiv:2401.04151*, 2024.
- [51] A. Yang, B. Yang, B. Zhang, B. Hui, B. Zheng, B. Yu, C. Li, D. Liu, F. Huang, H. Wei, et al. Qwen2. 5 technical report. *arXiv preprint arXiv:2412.15115*, 2024.
- [52] L. Zhang, L. Zhang, S. Shi, X. Chu, and B. Li. Lora-fa: Memory-efficient low-rank adaptation for large language models fine-tuning. *arXiv preprint arXiv:2308.03303*, 2023.
- [53] Y. Zhang, C. Chen, Z. Li, T. Ding, C. Wu, D. P. Kingma, Y. Ye, Z.-Q. Luo, and R. Sun. Adam-mini: Use fewer learning rates to gain more. *arXiv preprint arXiv:2406.16793*, 2024.
- [54] J. Zhao, Z. Zhang, B. Chen, Z. Wang, A. Anandkumar, and Y. Tian. Galore: Memory-efficient llm training by gradient low-rank projection. *arXiv preprint arXiv:2403.03507*, 2024.

- [55] Y. Zheng, R. Zhang, J. Zhang, Y. Ye, Z. Luo, Z. Feng, and Y. Ma. Llamafactory: Unified efficient fine-tuning of 100+ language models. In *Proceedings of the 62nd Annual Meeting of the Association for Computational Linguistics (Volume 3: System Demonstrations)*, Bangkok, Thailand, 2024. Association for Computational Linguistics.
- [56] H. Zhu, Z. Zhang, W. Cong, X. Liu, S. Park, V. Chandra, B. Long, D. Z. Pan, Z. Wang, and J. Lee. Apollo: Sgd-like memory, adamw-level performance, 2024.

Appendix for

Wavelet Meets Adam: Compressing Gradients for Memory-Efficient Training

A Experiment Details

A.1 Network Architecture

In this section, we describe the network architectures of the LLaMA (Large Language Model Meta AI) [42] and RoBERTa (Robustly Optimized BERT Approach) [25] models, which complement the experimental details provided in the main text. LLaMA is a family of foundational language models based on transformers [44]. For this paper, we adopt the LLaMA models from previous work [23], which use RMSNorm and SwiGLU activations [43, 42]. RoBERTa, on the other hand, is a variant of BERT (Bidirectional Encoder Representations from Transformers) [25], also built on the transformer architecture. Table 5 presents the architectural hyperparameters for the LLaMA and RoBERTa-base models, as well as the pre-training token amounts for LLaMA models across different sizes.

Table 5: Architecture hyperparameters of LLaMA for pre-training. Batch size and training data amount are specified in tokens.

Models	Params	Hidden	Intermediate	Heads	Layers	Iteration	Tokens
LLaMA	60M	512	1376	8	8	10K	1.3B
	130M	768	2048	12	12	20K	2.6B
	350M	1024	2736	16	24	60K	7.8B
	1B	2048	5461	24	32	100K	13.1B
	3B	2560	6848	32	32	120K	15.7B
RoBERTa	125M	768	3072	12	12	-	-

A.2 Experiment Hyperparameters

In this section, we provide detailed information on the hyperparameters and experimental setup used in the experiments discussed in the main text. For the LLaMA pre-training tasks, we follow the experimental configuration used in previous work [54], which employs the default Adam hyperparameters ($\beta_1 = 0.9, \beta_2 = 0.999, \epsilon = 10^{-6}$), a maximum sequence length of 256 tokens, and gradient accumulation with a batch size of 512. Additionally, we apply a learning rate warm-up for the first 10% of the iterations and use a cosine annealing schedule with the initial learning rate.

Table 6: Hyperparameter lr, α , training GPUs, and training time (hours) for different LLaMA models. We report the training time for Adam with our GWT.

	60M	130M	350M	1B
Full-Adam	0.005, -	0.001, -	0.001, -	0.0005, -
GWT	0.01, 0.25	0.01, 0.25	0.01, 0.25	0.01, 0.25
GaLore	0.01, 0.25	0.01, 0.25	0.01, 0.25	0.01, 0.25
APOLLO	0.01, 1.0	0.01, 1.0	0.01, 1.0	0.01, 1.0
GPUs (RTX 3090)	4	4	16	32
Time	0.99h	4.03h	11.83	40.18h

For the GWT method, we perform hyperparameter tuning on the scale parameter α from the set $[0.1, 0.15, 0.2, 0.25]$, selecting the value that yields the best performance across all LLaMA pre-training tasks. We found that our method is not sensitive to scale, and setting α to 0.25 yields good

results in most pretraining tasks, which is consistent with the hyperparameters used in previous work [54, 56]. For the baseline methods, we use their default hyperparameters: $\alpha = 0.25$ and $lr = 0.01$ for GaLore, and $lr = 0.001$ for Adam (0.0005 for Adam in LLaMA 1B and 3B). Consistent with prior work [54], we enable GWT and GaLore in the attention and MLP modules.

Finally, we summarize the hyperparameter α , the GPUs used (RTX 3090), and the training time (in hours) for our method required to reproduce the results shown of Table 1 in Table 6.

Table 7: Hyperparameter of different models on the MMLU benchmark.

Hyperparameters	Adam	LoRA	GaLore	APOLLO	GWT
Rank r	-	8	8	8	-
Level l	-	-	-	-	8
Scale α	-	16	2	32	0.25
lr scheduler			Cosine		
Warmup steps			10%		
Epochs			3		
Batch size w. accumulation			32		
Where			All		
N-shots			5		
Cut-off length			2048		
lr (LLaMA3.2-3B)	1.0e-6	2.5e-5	1.0e-5	1.0e-6	1.0e-5
lr (Gemma3-4B)	1.0e-6	5.0e-6	2.5e-6	1.0e-6	1.0e-5
lr (Qwen2.5-7B)	-	2.5e-6	2.5e-6	1.0e-6	5.0e-5

For the MMLU fine-tuning tasks, we adopt the implementation from [55] for both the dataset identity and the Alpaca English [40] with a max training sample. For our GWT method, we use a fixed decomposition level of $l = 8$ across all evaluated models. This setting aligns the memory footprint with low-rank-based baselines that employ a rank of 8. The gradient scaling coefficient α is empirically set to $\alpha = \frac{1}{2r}$. For other baselines, we follow the hyperparameter recommendations provided in their original papers: $\alpha = 2$ for GaLore [54], $\alpha = 32$ for APOLLO [56], and $\alpha = 16 (2 \times r)$ for LoRA [21]. In contrast to pre-training, we apply the memory-efficient fine-tuning technique to all linear layers during this task. We report the best accuracy obtained by sweeping the learning rate over the range [1.0e-6, 2.5e-6, 5.0e-6, 1.0e-5, 2.5e-5, 5.0e-5, 1.0e-4] for all the tested models fine-tuning. A summary of all used hyperparameters is provided in Table 7.

A.3 Experiment Enviroments

We utilize the BF-16 format throughout all pre-training processes to optimize memory usage. All experiments were conducted on a setup of 1 to 8 server nodes, each equipped with four NVIDIA 3090 GPUs and an Intel(R) Xeon(R) Gold 6226R CPU @ 2.90GHz. The Python version used is 3.10, with PyTorch [31] version 2.3.1 for pre-training and 2.6.0 for MMLU fine-tuning. For the implementation of GWT, we leverage the PyTorch Wavelet Toolbox [48].

A.4 Memory and Throughput Estimates

In this section, we provide further clarification on the GPU memory usage results reported in the paper. First, Table 8 presents the theoretical memory consumption of various methods for comparison.

Compared to low-rank methods that reduce memory overhead by controlling the rank, our Gradient Wavelet Transform (GWT) method does not require additional storage for projection matrices. Assuming the projection matrix size is negligible, GWT consumes approximately the same memory as projection-based methods such as GaLore and APOLLO. In practical experiments, GWT’s memory footprint is slightly **better** than these methods.

In actual training scenarios, GPU memory usage is influenced by multiple factors, including model size, batch size, optimizer states, PyTorch’s memory fragmentation management, and whether training

is conducted on a single GPU or across multiple GPUs. To focus on core differences, we estimate GPU memory usage for the model weights and Adam optimizer states using bfloat16 precision. For example, the weights of the LLaMA 60M model occupy approximately 0.12 GB of GPU memory, while the Adam optimizer states require about 0.23 GB. Since GWT primarily targets reducing optimizer memory usage, the weight memory footprint under Adam with GWT remains unchanged at 0.12 GB.

Regarding optimizer states, the memory consumption of the 2-level GWT matches that of GaLore, which uses a rank equal to one-quarter of the hidden size. In our experiments, both GWT and GaLore were applied exclusively to the attention and MLP modules of LLaMA, so the total optimizer memory usage depends on the number of parameters within these modules. Table 9 presents the estimated memory consumption for model weights and optimizer states across different methods and model configurations.

Table 8: **Memory comparison of different methods.** Suppose $W \in \mathbb{R}^{m \times n}$ ($m \leq n$), GaLore and LoRA adopt a rank of r , GWT applies a level of l .

	Full-Adam	GaLore	LoRA	GWT
Weights	mn	mn	$mn + mr + nr$	mn
Optimizer States	$2mn$	$mr + 2nr$	$2mr + 2nr$	$mn/2^{l-1}$
Pre-Training	✓	✓	✗	✓
Fine-Tuning	✓	✓	✓	✓

Besides the memory estimate, we also report the training throughput as a complement to the training speed report. For example, we pre-train LLaMA 60M with a total batch size of 512 and a max sequence length of 256 in 10,000 iterations. This is equivalent to a total token size of $512 \times 256 = 131072 \approx 131\text{K}$ and a total of $131072 \times 10000 = 1310720000 \approx 1.3\text{B}$ tokens during the whole training process. In Tables 12 and 6, we provide the training time and the number of GPUs used. Training LLaMA60M with our Haar-2 on four GPUs takes approximately 0.99 hours. Hence, we can compute the token throughput per GPU per second as $1310720000 / (0.99 \times 3600 \times 4) \approx 91.9\text{Ktokens/s}$

Table 9: **Memory estimate of weight parameters/optimizer states.** * indicates results published in prior works.

Methods	60M	130M	350M	1B
Full-Rank*	0.12G/0.23G	0.25G/0.51G	0.68G/1.37G	2.60G/5.20G
GWT-2	0.12G/0.12G	0.25G/0.27G	0.68G/0.54G	2.60G/1.78G
GWT-3	0.12G/0.10G	0.25G/0.23G	0.68G/0.40G	2.60G/1.21G
GaLore-1/4	0.12G/0.12G	0.25G/0.27G	0.68G/0.54G	2.60G/1.78G
GaLore-1/8	0.12G/0.10G	0.25G/0.23G	0.68G/0.40G	2.60G/1.21G
Low-Rank*	0.08G/0.17G	0.18G/0.37G	0.36G/0.72G	1.19G/2.38G
LoRA*	0.20G/0.17G	0.44G/0.37G	1.04G/0.72G	3.79G/2.38G
ReLoRA*	0.20G/0.17G	0.44G/0.37G	1.04G/0.72G	3.79G/2.38G

B Fine-tuning on GLUE

For a more comprehensive comparison with GaLore and to assess GWT’s performance across more tasks, we fine-tune a pretrained RoBERTa-base model on the GLUE benchmark. We report performance metrics across various tasks: overall accuracy (matched and mismatched) for MNLI, Matthew’s correlation for CoLA, Pearson correlation for STS-B, F1 score for MRPC, and accuracy for the remaining tasks. We present the best results for all methods after tuning the learning rate. We present the corresponding experimental results in Table 10. Compared to GaLore and APOLLO, GWT shows a smaller gap from the full-rank baseline.

For the GLUE fine-tuning tasks, we set the α hyperparameter to 2 for both GWT and GaLore (enable GWT and GaLore in all modules). The lr for GWT is chosen from the interval $[1 \times 10^{-6}, 1 \times 10^{-5}]$, GaLore is tuned within the interval $[5 \times 10^{-6}, 5 \times 10^{-5}]$. For each GLUE task, we use a batch size of 16 (except for CoLA, where the batch size is 32), train for 30 epochs, and set the maximum sequence length to 512. All experiments were conducted using a PyTorch [31] random seed of 1234 to ensure reproducibility.

Table 10: **Fine-tuning on GLUE benchmark using pre-trained RoBERTa-Base model.** We present the final validation and average scores for all tasks (higher is better).

	CoLA	STS-B	MRPC	RTE	SST2	MNLI	QNLI	QQP	Avg.
Adam	63.81	91.26	92.25	79.06	94.57	87.29	92.18	92.28	86.58
GaLore	61.32	91.13	92.41	77.25	94.03	86.77	92.56	91.77	85.90
APOLLO	61.07	90.70	92.00	78.33	93.57	87.21	92.27	91.85	85.87
LoRA* [54]	61.83	90.80	91.90	79.06	93.46	86.94	92.25	91.22	85.93
GWT	62.57	91.16	93.26	79.42	94.26	87.37	92.53	91.94	86.56

Table 11: GLUE benchmarks scores with different learning rates for GWT. We present the used learning rate for the results in Table 10.

	CoLA	STS-B	MRPC	RTE	SST2	MNLI	QNLI	QQP
1E-06	57.01	90.19	90.55	76.17	94.03	86.95	92.45	91.46
2E-06	58.29	90.70	91.87	78.70	-	-	-	-
3E-06	59.81	91.07	92.09	79.42	93.92	87.07	92.51	91.84
4E-06	62.07	90.94	91.16	78.33	-	-	-	-
5E-06	62.57	91.16	93.18	75.81	94.26	87.37	92.53	91.81
6E-06	62.07	90.97	92.76	78.70	-	-	-	-
7E-06	59.43	90.70	92.36	73.64	94.15	97.35	92.38	91.94
8E-06	59.81	90.93	91.73	77.25	-	-	-	-
9E-06	59.30	90.84	93.26	77.25	92.31	86.84	92.30	91.78
1E-05	59.57	90.75	91.79	78.70	-	-	-	-
lr	5e-06	5e-06	9e-06	3e-06	5e-06	5e-06	5e-06	7e-06
Batch size	32	16	16	16	16	16	16	16

C Hyperparameter Study

In addition to the hyperparameters required by the original optimizer, several additional hyperparameters are needed to apply our GWT method. The hyperparameter α stands for the scale factor. Specifically, the scale hyperparameter α determines the magnitude of the update for the GWT module of $\eta \cdot \alpha$ (η for the modules without GWT). The H, \tilde{H} hyperparameters depend on the GWT basis used in the process (e.g., Haar, DB2, Rbio2.6, etc.). The choice of filter impacts the transformation applied during the wavelet decomposition and reconstruction. l stands for the GWT level, 1 denotes 1-level GWT which can reduce the optimizer memory up to 50%, and 2 denotes 2-level GWT which reduces the memory usage up to 75%, respectively. These levels allow for varying degrees of memory reduction depending on the depth of the wavelet decomposition applied. Larger l can bring higher memory reduction but influence the throughput. These additional hyperparameters allow for more flexibility in applying GWT to different optimization problems while controlling the trade-off between memory usage and update precision. In this section, we investigate the effects of the hyperparameters α and GWT level l .

Scale α . We evaluate Adam with 2-level Haar GWT using different values of α at a fixed learning rate ($lr = 0.01$). As shown in Figure 6(a) and 6(b), we observe that our GWT is invariant to the

hyperparameter. For α values larger than 0.1, the final experimental results remain relatively stable and do not differ significantly. Based on the network initialization strategy we used, most modules in the network have a learning rate greater than 0.001 ($lr \times \alpha$). In contrast to Adam, which often requires a learning rate smaller than 0.001 to avoid loss spikes, GWT shows significantly better robustness to higher learning rates. For fine-tuning tasks, tuning α is equivalent to adjusting the learning rate (lr) hyperparameter based on our strategy. A detailed study of the learning rate hyperparameters (lr, α) on fine-tuning tasks is presented in Appendix A.2.

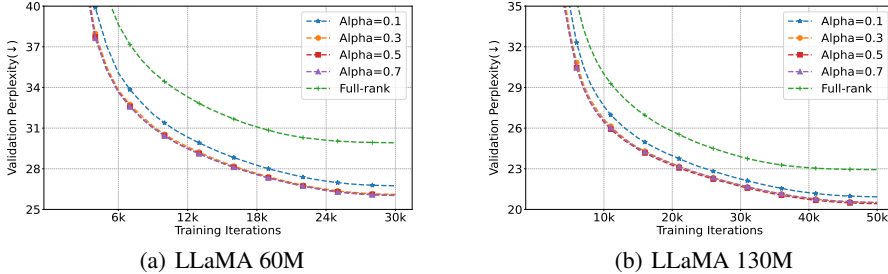


Figure 6: Study the effects of α on pre-training LLaMA 60M and 130M models.

GWT level l . We investigate the effects of the GWT level hyperparameter l , with the corresponding validation perplexity curves shown in Figure 5. We found that the value of l has little impact on the final experimental results, and lower values of l are only slightly better than others. One question that arises from the experimental results is whether the approximation coefficients are not crucial when using wavelets to compress gradients in LLM training, but rather the detail coefficients. The main impact of l seems to be on memory usage and throughput. The throughput results and optimizer memory estimate for different GWT levels are summarized in Table 12, demonstrating the trade-off between memory efficiency and model performance. Higher wavelet levels improve memory usage, but this may come at the cost of slightly higher validation perplexity and slower training speed.

Table 12: Estimated optimizer memory usage and token throughput (per GPU) with different GWT levels. Higher GWT levels lead to slower training token throughput but smaller memory usage.

Methods	60M		130M		350M	
	Memory	Tokens/s	Memory	Tokens/s	Memory	Tokens/s
GWT-1	0.16G	95.8K	0.36G	46.0K	0.81G	12.7K
GWT-2	0.12G	91.9K	0.28G	45.1K	0.54G	12.1K
GWT-3	0.10G	90.1K	0.24G	44.8K	0.40G	11.5K
GWT-4	0.09G	84.2K	0.22G	43.8K	0.33G	10.8K
GWT-5	0.08G	83.5K	0.21G	41.5K	0.29G	9.25K

Wavelet filter H . In the main text, our GWT method uses the Haar wavelet basis by default. Different wavelet bases capture information in distinct ways, which can result in variations in compression performance. To investigate the impact of different wavelet bases, we evaluated GWT’s pretraining performance and memory overhead using several orthogonal wavelet bases, including Bior (Biorthogonal Wavelets), SYM (Symmetric Wavelets), and Coif (Coiflets). The experimental results, presented in Table 13, show that the choice of wavelet basis has minimal effect on the overall experimental outcomes.

D Adam with Module-wise Learning Rate

One key learning rate strategy employed in GWT is the assignment of different learning rates to distinct parameter modules. Specifically, the overall learning rate is partitioned such that the Attention and MLP modules are updated using a scaled learning rate of $lr \times \alpha$, while the rest of the model

Table 13: Access GWT with different wavelet bases. “Haar-2” refers to GWT with a 2-level discrete Haar wavelet transform. The symbol “+” indicates that the memory usage is slightly higher than the estimated value.

Wavelet	60M	130M
Haar-2	29.35 (0.24G)	22.47 (0.52G)
DB-2	29.60 (0.24G+)	22.59 (0.52G)
Bior-2	29.34 (0.24G+)	22.37 (0.52G+)
SYM-2	29.42 (0.24G)	22.45 (0.52G)
Coif-2	29.24 (0.24G+)	22.40 (0.52G)

uses the base learning rate lr . This modular learning rate strategy is commonly adopted in memory-efficient training algorithms, including LoRA [21], GaLore [54], Fira [6], and APOLLO [56]. We incorporate this strategy into GWT as a standard configuration. The method of using different learning rates for different network modules in Adam optimizer has been studied in related works [12, 14]. Here, we provide a supplement as an additional ablation experiment to the original text.

In this section, we first apply the same modular learning rate scheme to the Adam optimizer to examine whether it also benefits from this design, and to evaluate whether GWT can still match or surpass Adam’s performance, as demonstrated in the main text. Following standard practice in other memory-efficient methods, we use a learning rate of $lr \times \alpha$ for the Attention and MLP modules, while keeping lr for the remaining modules. To measure the benefit of this configuration, we compare it with Adam using a unified learning rate of $2.5e-3$, selected from the range $[1e-3, 2.5e-3, 5e-3, 7.5e-3, 1e-2]$ based on best performance. The learning curves are shown in Figure 7. We then apply a uniform learning rate ($\alpha = 1.0$) to GWT and evaluate its performance under this setting, with results reported in Figure 8.

Experimental results show that, under our setup, Adam significantly benefits from the modular learning rate strategy, achieving clearly better performance than with a single global learning rate. Even with this enhanced setting, GWT achieves a final validation perplexity (PPL) close to that of Full-Adam. This partly explains why many memory-efficient training methods can outperform full-rank Adam—the modular learning rate strategy plays a key role. It also suggests that Attention and MLP modules may require smaller learning rates than other parts of the model. These findings raise an important question: Do different modules in LLMs inherently demand distinct learning rates? And could explicitly integrating modular learning rate strategies into Adam lead to further gains?

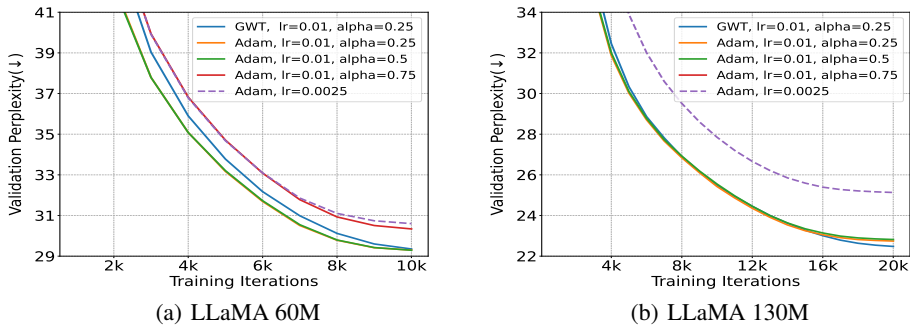


Figure 7: **Applying module-wise learning rate to Adam optimizer.** We can observe that applying a module-wise split learning rate in Adam leads to better convergence speed and final results compared to using a uniform learning rate across all modules.

E Discussion

Our proposed GWT and its implementation draw inspiration from GaLore [54]. Both GWT and GaLore are closely related to Projected Gradient Descent (PGD) [4, 7], which projects the gradient

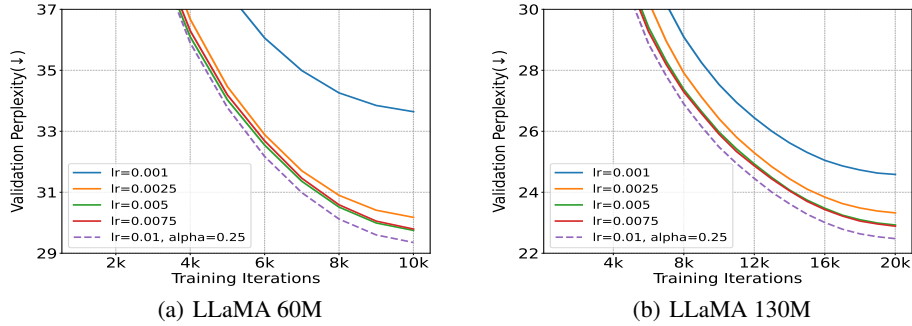


Figure 8: **Applying same learning rate to all modules for GWT optimizer.** Similar to Adam, the module-wise learning rate yields better experimental performance compared to using a unified learning rate.

onto a subspace before performing the update. However, there are key distinctions between GWT and GaLore. The primary difference lies in the projection operation: GWT not only projects the gradient onto the subspace but also leverages additional information from this projection, such as the detail coefficients D_t (as shown in Eq. (6)). In contrast, GaLore discards the remaining information after projecting the gradient onto the subspace. When projecting back from the subspace to the gradient space, GWT retains more of the original gradient information. Importantly, this additional information is temporary and generated during the wavelet transform process itself, so it does not require extra storage. In summary, GWT provides an effective solution to the memory challenges encountered in training large models.

Here, we outline several intriguing open problems related to GWT: (a) The theoretical foundations behind GWT’s effectiveness in training remain unexplored. A deeper analysis of the method’s convergence and the limitations associated with its use is critical for refining its application and gaining a more comprehensive understanding of its behavior within optimization frameworks. (b) The wavelet transform operations themselves still require optimization. Wavelets were originally designed for time-series signals and images, raising the question: Can a specialized wavelet transform be developed to handle gradients, which are inherently more disordered and chaotic? Additionally, since the impact of l on the experimental results is minimal, the main effect of higher-order GWT lies in throughput, while offering higher memory efficiency. Therefore, the potential of GWT with higher l values is worth exploring. Given the linear properties of the Haar wavelet in GWT, is it possible to accelerate multi-level wavelet transforms to achieve even higher memory compression ratios, such as 1/64 or 1/128? (c) Finally, the applicability and effectiveness of GWT in other domains, such as vision models [11, 26] and diffusion models [19, 39], remain to be validated.

F General Optimizer with GWT

In general, backpropagation in deep learning training follows the update rule:

$$W_{t+1} = W_t - \eta \cdot \sum_{k=1}^t \tau_k(G_k), \quad (7)$$

where τ_k is a gradient regularizer dependent on optimizer states, which include state updates. Specifically, τ_k serves as an abstract representation of both first-order momentum and second-order momentum in Adam.

Building on the operation from the previous section, we first apply a GWT to the gradient G_k , yielding A_k and D_k (Eq. (2)). By substituting A_k into the optimizer state update and performing a reverse wavelet transform (multiply by \tilde{H}), we can naturally incorporate the GWT into the optimizer and the corresponding states. The update recursion with GWT can then be written as:

Algorithm 2 General optimizer with GWT

Input: Weight matrix W , step size η , batch size m , regularizer τ_t , iteration T , transform level l , scale factor α , iteration T , wavelet transformer H, \tilde{H} .

Initialize $t \leftarrow 0$

repeat

$$G_t \leftarrow \frac{1}{m} \sum_{i=1}^m \nabla_W f_i(W_t)$$

$$A_t, D_t \leftarrow G_t \tilde{H}$$

$$\tilde{A}_t \leftarrow \sum_{k=1}^t \tau_k(A_t)$$

$$\tilde{G}_t \leftarrow [\tilde{A}_t, D_t] \tilde{H}$$

$$W_t \leftarrow W_{t-1} + \eta \cdot \tilde{G}_t$$

until $t = T$

return W_t

▷ Gradient wavelet transform

▷ State update

▷ Reverse transform

$$W_{t+1} = W_t - \eta \cdot \left[\sum_{k=1}^t \tau_k(A_k), D_t \right] \tilde{H}. \quad (8)$$

This equation captures the integration of wavelet transform-based adjustments into the optimizer’s update rule. To this end, we have developed a unified update schedule for optimizers with GWT based on linear formulation and demonstrated that GWT can be directly applied to existing optimizers with heavy-state memory usage. Therefore, we incorporate our GWT into Adam-mini [53] and MUON [24] optimizers for LLaMA pre-training tasks, and present the experimental results in Figure 4.

G Benchmark Details

In this section, we provide a detailed description of the benchmarks used in the paper, serving as a supplement to the results section 4.

C4 benchmark. We adopt the Colossal Clean Crawled Corpus (C4) [34] benchmark of the English version for all the pre-training tasks. The C4 English benchmark is a colossal, cleaned version of Common Crawl’s web crawl corpus based on the Common Crawl dataset. Includes 305GB of English-language text and is mainly intended to pre-train language models. The validation complexity is obtained by taking the validation loss and exponentiating it with the base of Euler’s number e .

MMLU Benchmark. We evaluate the performance of LLaMA3.2-3B [15], Qwen2.5-3B [51], and Gemma3-4B [41] on the Multi-task Language Understanding (MMLU) benchmark [18]. The MMLU benchmark is designed to assess the knowledge acquired by models during pretraining, focusing on their performance in zero-shot and few-shot settings. It spans 57 subjects, including areas in STEM, the humanities, social sciences, and more.

GLUE benchmark. We fine-tune RoBERTA-base model [25] on General Language Understanding Evaluation (GLUE) [45] benchmark. GLUE is a collection of resources for training, evaluating, and analyzing natural language understanding systems, including CoLA (The Corpus of Linguistic Acceptability, binary classification) [46], STS-B (Semantic Textual Similarity Benchmark, textual similarity regression) [3], MRPC (Microsoft Research Paraphrase Corpus, paraphrase detection) [10], RTE (Recognizing Textual Entailment, inference task), SST2 (Stanford Sentiment Treebank, sentiment analysis) [38], MNLI (Multi-Genre Natural Language Inference Corpus, textual entailment task) [47], QNLI (Stanford Question Answering Dataset, inference task) [36], QQP (question answering). The broad coverage makes GLUE a standard benchmark for evaluating pre-training BERT models [21].